





Research Article

Nonlinear Observer-Based Control Design for a Three-Axis Inertial Stabilized Platform

Mohammad Mehdi Zohrei¹ , and Hamidreza Javanmardi^{2,*} 

¹ Department of Electrical and Electronic Engineering, Shiraz University of Technology, Shiraz 71557-13876, Iran

² School of Electrical and Computer Engineering, Shiraz University, Shiraz, Iran

* Corresponding Author: hamidjavanmardi@shirazu.ac.ir

Abstract: For decades in the aerospace and control sciences, the Inertial Stabilized Platform (ISP) system has been studied to improve the accuracy of recipient photos or target tracking. This paper presents a nonlinear observer-based control method for three Degrees Of Freedom (3-DOF) ISP systems. First, a new formula of the state space equation for the 3-DOF ISP system is proposed to make this model suitable for designing an observer-based control. Then, by measuring the angular positions as output feedback, the angular velocities are estimated by the nonlinear observer, and Lyapunov-based nonlinear control techniques are used to design the observer. Furthermore, the exponential stability and convergence of the observer system are proved. Finally, the auxiliary control signal is considered so that the dynamics of the designed observer become a simple linear form and are easily controlled by the state feedback controller. Simulation results illustrate the effectiveness and feasibility of the proposed control strategy.

Keywords: Exponential stability, inertial stable platform, lyapunov techniques, observer-based control, state feedback controller.

Article history

Received 01 February 2023; Revised 09 October 2023; Accepted 17 November 2023; Published online 29 January 2024.

© 2024 Published by Shahid Chamran University of Ahvaz & Iranian Association of Electrical and Electronics Engineers (IAEEE)

How to cite this article

M. M. Zohrei, and H. Javanmardi, "Nonlinear observer-based control design for a three-axis inertial stabilized platform," *J. Appl. Res. Electr. Eng.*, vol. 2, no. 2, pp. 158-172, 2023. DOI: [10.22055/jaree.2023.42938.1066](https://doi.org/10.22055/jaree.2023.42938.1066)



1. INTRODUCTION

1.1. Motivation

Recently, receiving photos with high accuracy and quality from a moving target have received a lot of attention. Noise and disturbances from cameras and sensors mounted on moving vehicles such as airplanes, helicopters, boats, etc. have adverse effects and interfere with access to high-precision photos [1–3]. For this reason, the Inertial Stabilized Platform (ISP) is used to improve the accuracy of the recipient's photo or target tracking. The ISP plant is one of the most important parts of the inertial technology application system with broad applications in submarines, electronic telescopes, boats, satellites, helicopters, and spacecraft [4–7]. The ISP system including gimbals is used to isolate the movement of several cameras and sensors from changes in the angular position of the moving object [8]. Therefore, using this system, the accuracy of imaging and tracking the target is improved [9]. Moreover, various noises and disturbances exist, including internal disturbances such as mass imbalance torque, sensors measurement error and

friction force, and external disturbances generated by wind disturbances or moving items' motion and vibration [10]. In addition, the state space equation of the ISP system is very complex and has nonlinear dynamics. These statements show that achieving optimal performance control for the ISP system is challenging and has received much attention in recent decades [11].

1.2. Literature review

To improve the ISP plant performance, several control techniques have been suggested in the literature. In [12], a Proportional-Integral-Derivative (PID) controller is combined with a fuzzy technique to control the ISP system, although this method is not robust against disturbances and the controller performance is degraded against strong perturbations. Moreover, the performance of conventional PID controllers can be improved by combining them with the Neural Network approach [13, 14]. The backstepping technique is also suggested in some literature [15] but, it does not have satisfactory performance in the presence of disturbances and system uncertainties. To improve the control

performance against disturbances and uncertainties in the system, the controller must be robust. Therefore, several researchers have contributed to this field [16–18]. In [19–22], the H_∞ feedback controller is designed to be robust to various uncertainties and disturbances and has good performance. The nonlinear model predictive control is another efficient and robust controller that recently has been used for ISP systems [1, 23]. A sliding mode controller is also one of the most popular controller design techniques for the ISP system [24]. To improve the control performance, a combination of sliding mode techniques and a backstepping controller is widely used [25, 26]. Despite the advantages of this method, the sliding mode controller has a heavy switching gain, which causes chattering in the input signal control. The high switching in the control effort may damage the actuating motors to control the ISP system. In [8, 25], to decrease the chattering effect, the neural network approach has been used to estimate the disturbances imposed on the system. However, neural network training is usually time-consuming and can lead to weak transient performance in some complex systems. In addition, in all examined control techniques for ISP systems, it is assumed that all system variables are available and measurable. Whereas, in most practical systems, measuring all states of the system by direct observation is very costly and is usually accompanied by errors. An observer-based control design is one of the efficient approaches for accurately estimating the state of the ISP axis because it is simple and very applicable [27, 28]. Only a model of the desired system is required to design the observer. When an accurate numerical model of the plant is provided, the velocity observer can estimate an accurate steady state of the system. However, in dealing with an unknown real system model, various uncertainties and disturbances are always modeled, therefore accurate estimation of states is not so easy and also cannot be guaranteed [28, 29]. In the works of literature, various methods for estimating system states and then designing an observer-based controller are introduced. Such as extended state observer [30, 31], backstepping observer [32, 33], disturbance observer [34], and unknown input observer [35]. Also, in [36] the observer-based integral sliding mode control (SMC) for a class of stochastic linear flight systems subject to bounded disturbances is suggested. In [37], an adaptive observer design problem to estimate the parameters and state variables of Lipschitz systems has been investigated. The observer designed in [37] is suitable for systems that are non-linear in state variables and linear in unknown parameters. Also, the problem of designing a nonlinear adaptive observer for Lipschitz systems has been expanded in [38]. The gain for this nonlinear observer is systematically obtained using the linear matrix inequality technique.

1.3. Contributions

In this paper, an efficient simple-implementation observer-based controller method is proposed for a 3-DOF ISP system. To control the ISP system, in addition to angular positions, angular velocities with appropriate accuracy are required. However, high-precision gyroscopes are generally costly, and in addition, gyroscope rate drift often causes errors over time [39]. To reduce the above-mentioned problem of velocity gyros, the velocity observer is used to estimate the vector of velocity based on the Lyapunov theorem. For this purpose, first, using the kinetics and

kinematics of the ISP, the dynamic equations of each gimbal activated by the DC motor are obtained. Then the state variables of the ISP system are divided into two categories of angular position and angular velocity, and the state space equations are rewritten in a form that is suitable for designing a velocity observer. Next, with the help of Lyapunov-based nonlinear control techniques, a nonlinear observer is designed to improve the velocity estimation for the roll, pitch, and yaw gimbal of the ISP plant. By using the Lyapunov theorem, the overall ISP system stabilization and moving target tracking are guaranteed. Finally, the auxiliary control signal is considered in such a way that the dynamics of the designed observer become a simple linear form and is easily controlled by the state feedback controller. The suggested method is applied to the 3-DOF ISP case study, and the simulation results have shown the improvement of the designed controller.

Briefly, the presented paper has the following contributions and advantages over the current literature:

- i. Initially, a new formulation of the state-space equation is proposed for the 3-DOF ISP system so that this model is suitable for designing an observer-based control. For the designed controller to be robust against model uncertainties and external disturbances, the term of unknown bounded nonlinear disturbance in the ISP model is also considered in the driven model.
- ii. In almost all control strategies presented in the various literature for ISP systems, it is assumed that all system state variables with appropriate accuracy are available. However, one of the biggest challenges in the practical design of controllers for ISP systems, in addition to the issue of cost limitation and accuracy of measuring devices that always have errors, is the volume and weight added to the overall system. Therefore, in this paper, to improve the performance of the designed controller as well as reduce the implementation costs, it is assumed that the position vector θ is available and measurable but the angular velocity vector ω is not available which must be estimated. Therefore, it is no longer necessary to use expensive gyroscopes to directly measure the angular velocity, and an observer is used instead.
- iii. By using the state observer, one of the most important parts of the design is to prove the convergence of the estimated value to the actual value. In this paper, with the help of Lyapunov's theorem and by considering a new positive definite function, it is guaranteed that the state estimation error converges to zero asymptotically.
- iv. The suggested controller strategy is very simple and its implementation requires a low computational burden.

1.4. Paper Structure

The structure of the sections of this paper is as follows: in Section 2, the dynamic model of the 3-DOF ISP system is obtained and a suitable state space model for designing the velocity observer is derived. Section 3 presents the observer-based control method for the 3-DOF ISP plant and the exponential stability analysis. The simulation results are illustrated to show the effectiveness of the proposed method in Section 4. Finally, this paper is concluded in Section 5.

2. DYNAMIC OF 3-DOF ISP

Fig. 1 presents the configuration of the 3-DOF ISP plant which consists of the torque motor, outer loop (roll gimbal), middle loop (pitch gimbal), and inner loop (yaw gimbal). The imaging sensors and payloads are placed on the inner loop (yaw gimbal), and the position and orientation system (POS) is placed on the pitch gimbal to provide attitude-measured information for the rotation angles of the gimbal and ensure accurate pointing of the imaging sensors. In this section, first, the corresponding coordinate systems are defined and then a method for converting vectors from one coordinate system to another is introduced. The coordinate system of the 3-DOF ISP plant is shown in Fig. 1. By using Euler angles, the position of a fixed point can be defined as vector $\theta_A = [\theta_p \ \theta_r \ \theta_a]^T$, which (θ_p) is the position of the pitch angle, (θ_r) is a position of the roll angle, and (θ_a) is the position yaw angle. Moreover, roll-pitch-yaw velocities relating to the base coordinate are defined as vector $\dot{\theta}_A = [\dot{\theta}_p \ \dot{\theta}_r \ \dot{\theta}_a]^T$.

In Fig. 2 (x_r, y_r, z_r) , (x_a, y_a, z_a) , (x_p, y_p, z_p) and (x_b, y_b, z_b) are the roll coordinate, yaw coordinate, pitch coordinate, and base coordinate respectively.

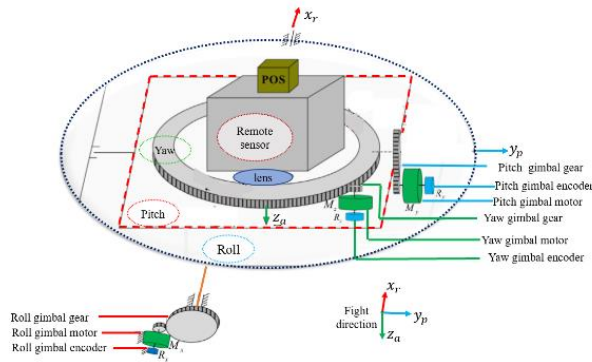


Fig. 1: The 3-DOF ISP configuration diagram [8].

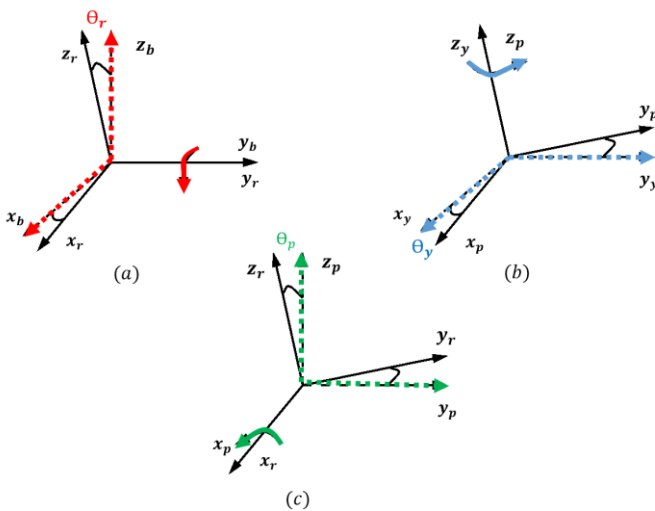


Fig. 2: coordinates of 3-DOF ISP plant: (a) roll gimbal, (b) yaw gimbal, (c) pitch gimbal.

2.1. Kinematics Model of the 3-DOF ISP Plant

According to Fig. 2, C_b^r , C_r^p , and C_p^a are transformation matrices from the base coordinate of the gimbal to the roll coordinate, the roll coordinate of the gimbal to the pitch coordinate, and the pitch of the gimbal coordinate to the yaw coordinate respectively defined as follows:

$$C_b^r = \begin{bmatrix} \cos(\theta_r) & 0 & -\sin(\theta_r) \\ 0 & 1 & 0 \\ \sin(\theta_r) & 0 & \cos(\theta_r) \end{bmatrix} \quad (1)$$

$$C_r^p = \begin{bmatrix} 1 & 0 & 0 \\ 0 & \cos(\theta_p) & \sin(\theta_p) \\ 0 & -\sin(\theta_p) & \cos(\theta_p) \end{bmatrix} \quad (2)$$

$$C_p^a = \begin{bmatrix} \cos(\theta_a) & \sin(\theta_a) & 0 \\ -\sin(\theta_a) & \cos(\theta_a) & 0 \\ 0 & 0 & 1 \end{bmatrix} \quad (3)$$

According to the defined transformation matrices (1)-(3), the kinematics of the 3-DOF ISP plant in different coordinates are given as follows [8]:

$$\omega_{ir}^r = \begin{bmatrix} \omega_{irx}^r \\ \omega_{iry}^r \\ \omega_{irz}^r \end{bmatrix} = C_b^r \omega_{ib}^b + \begin{bmatrix} \dot{\theta}_r \\ 0 \\ 0 \end{bmatrix} \quad (4)$$

$$\omega_{ip}^p = \begin{bmatrix} \omega_{ipx}^p \\ \omega_{ipy}^p \\ \omega_{ipz}^p \end{bmatrix} = C_r^p \omega_{ir}^r + \begin{bmatrix} \dot{\theta}_p \\ 0 \\ 0 \end{bmatrix} \quad (5)$$

$$\omega_{ia}^a = \begin{bmatrix} \omega_{iax}^a \\ \omega_{ia y}^a \\ \omega_{iaz}^a \end{bmatrix} = C_p^a \omega_{ip}^p + \begin{bmatrix} 0 \\ 0 \\ \dot{\theta}_a \end{bmatrix} \quad (6)$$

where $\omega_{ir}^r = [\omega_{irx}^r \ \omega_{iry}^r \ \omega_{irz}^r]^T$, $\omega_{ip}^p = [\omega_{ipx}^p \ \omega_{ipy}^p \ \omega_{ipz}^p]^T$, $\omega_{ia}^a = [\omega_{iax}^a \ \omega_{ia y}^a \ \omega_{iaz}^a]^T$, and $\omega_{ib}^b = [\omega_{ibx}^b \ \omega_{iby}^b \ \omega_{ibz}^b]^T$ are the angular velocity vector in directions (x, y, z) of the roll-pitch-yaw and base, relative to the inertial coordinate, respectively.

2.2. The Dynamic Model of the 3-DOF ISP Plant

According to Newton–Euler theory, the dynamic model of the 3-DOF ISP plant can be written as follows [8]:

$$\dot{H}_k + \omega_k \times H_k = M_k, \quad k = a, p, r \quad (7)$$

In equation (7), $\omega_k = [\omega_{kx} \ \omega_{ky} \ \omega_{kz}]^T$ is defined as the vector of angular velocity and $H_k = [H_{kx} \ H_{ky} \ H_{kz}]^T$ is the vector of the angular momentum of inertia for the roll-pitch-yaw gimbal. In the following, the inertial angular momentum concerning the coordinates of inertia and the dynamic model of the roll, pitch, and yaw gimbal is defined.

2.2.1. The angular momentum of inertia and dynamic model of the pitch gimbal

The inertial angular momentum of the pitch gimbal is given as follows:

$$H_p = J_p \omega_{ip}^p + C_a^p H_a = \begin{bmatrix} (J_{px} + J_{ax}) \omega_{ipx}^p \\ (J_{py} + J_{ay}) \omega_{ipy}^p \\ (J_{pz} + J_{az}) \omega_{ipz}^p + J_{az} \dot{\theta}_a \end{bmatrix} \quad (8)$$

By substituting H_p and ω_{ip}^p to equation (7), the dynamic model of the pitch gimbal is defined by

$$\begin{aligned} & \left((J_{px} + J_{ax}) \omega_{ipx}^p \right)' \\ & + (J_{pz} + J_{az} - J_{py} - J_{ay}) \omega_{ipy}^p \omega_{ipz}^p + J_{az} \dot{\theta}_a \omega_{ipy}^p \\ & = M_{px} \end{aligned} \quad (9)$$

2.2.2. The angular momentum of inertia and dynamic model of the roll gimbal

The inertial angular momentum of the roll gimbal is given as follows:

$$H_r = J_r \omega_{ir}^r + C_p^r H_p \quad (10)$$

By substituting H_r and ω_{ir}^r to equation (7), the dynamic model of the roll gimbal is defined by

$$\begin{aligned} & [J_{ry} \omega_{iry}^r + (J_{py} + J_{ay}) \omega_{ipy}^p \cos \theta_p - J_{az} \dot{\theta}_a \sin \theta_p \\ & \quad - \sin \theta_p (J_{az} + J_{pz}) \omega_{ipz}^p] \\ & + (J_{rx} - J_{rz}) \omega_{irx}^r \omega_{irz}^r + (J_{ax} + J_{px}) \omega_{ipx}^p \omega_{irz}^r \\ & \quad - \sin \theta_p (J_{py} + J_{ay}) \omega_{ipy}^p \omega_{irx}^r \\ & - \cos \theta_p (J_{az} + J_{pz}) \omega_{ipz}^p \omega_{irx}^r \\ & \quad - \cos \theta_p J_{az} \dot{\theta}_a \omega_{irx}^r = M_{ry} \end{aligned} \quad (11)$$

2.2.3. The angular momentum of inertia and dynamic model of the yaw gimbal

The inertial angular momentum of the roll gimbal is given as follows:

$$H_a = J_a \omega_{ia}^a \quad (12)$$

By substituting H_a and ω_{ia}^a to equation (7), the dynamic model of the roll gimbal is defined by

$$J_{az} \dot{\omega}_{iaz}^a = M_{az} \quad (13)$$

where in the above equation, J_{mn} is the rotary momentums of the m gimbal around the n-axes.

Moreover, a DC motor with a gear-driven transmission is provided to generate the torque required to control the 3-DOF ISP plant. The dynamic equations of a gimbal gear-driven plant are considered as follows [8]:

$$\begin{cases} M_L = R_L F + T_{dL} \\ J_m \frac{d^2 \theta_{im}}{dt^2} = T_M - R_m F + T_{dm} \end{cases} \quad L = a, p, r \quad (14)$$

where, M_L is the torque applied on the gimbal, R_m is the armature resistance, T_{dL} is the total disturbance torque imposed on the gimbal, F is the interacting force between the two gears, J_m is the motor inertial, θ_{im} , θ_{iL} and θ_{ir} are the attitudes of the motor, gimbal, and reference concerning the inertial space, respectively. Also T_M is the output torque of the motor is defined as follows:

$$T_M = K_t \frac{u - K_e (\dot{\theta}_{im} - \dot{\theta}_{ib})}{R_m} \quad (15)$$

In equation (15), K_t represents the motor torque constant, and K_e is known as the back Electromotive Force (EMF) constant. Moreover, the torque applied on each gimbal (M_L) is defined as follows:

$$M_L = NK_t \frac{u - K_e (\dot{\theta}_{iL} - \dot{\theta}_{ib})}{R_m} + (NT_{dm} + T_{dL}) + N(N-1)J_m \dot{\theta}_{ib} - N^2 J_m \ddot{\theta}_{iL} \quad (16)$$

By substituting (4)-(7) and (14) in (8)-(13), the dynamic model of the 3-DOF ISP plant with a DC motor and a gear-driven transmission for pitch, roll, and yaw is obtained as follows

$$\begin{aligned} & (J_{px} + J_{ax}) \omega_{ipx}^p \ddot{\theta}_p \\ & = -(J_{px} + J_{ax}) \dot{\omega}_{irx}^r \\ & \quad + J_{az} \dot{\theta}_a \omega_{ipy}^p \\ & \quad + (J_{pz} + J_{az} - J_{py} - J_{ay}) \omega_{ipy}^p \omega_{ipz}^p \\ & \quad + \frac{NK_t}{R_m} (u_p \\ & \quad - K_e N (\dot{\theta}_{ip}^p - \omega_{ibx}^a)) \\ & \quad + NT_{dm} + T_{dp} \\ & \quad + N(N-1)J_m \dot{\omega}_{ibx}^p \\ & \quad - N^2 J_m \ddot{\theta}_{ip}^p \end{aligned} \quad (17)$$

$$\begin{aligned} & (J_{ry} + \cos^2(\theta_p) (J_{ay} + J_{py})) \ddot{\theta}_r \\ & = \dot{\theta}_r \cos^2(\theta_p) \\ & \quad + (J_{ay} + J_{py}) \cos^2(\theta_p) \omega_{iby}^b \\ & \quad + (J_{ay} + J_{py}) \cos(\theta_p) \sin(\theta_p) \omega_{irz}^r \\ & \quad - (J_{az} + J_{pz}) \sin(\theta_p) \omega_{ipz}^p \\ & \quad - J_{az} \sin(\theta_p) \dot{\theta}_a \\ & \quad + (J_{rx} - J_{rz}) \omega_{irx}^r \omega_{irz}^r \\ & \quad + (J_{ax} + J_{px}) \omega_{ipx}^p \omega_{irz}^r \\ & \quad - (J_{ay} + J_{py}) \sin(\theta_p) \omega_{ipy}^p \omega_{irx}^r \\ & \quad - (J_{az} + J_{pz}) \cos(\theta_p) \omega_{ipz}^p \omega_{irx}^r \\ & \quad - J_{az} \cos(\theta_p) \dot{\theta}_a \omega_{irx}^r \\ & \quad + \frac{NK_t}{R_m} (u_r \\ & \quad - K_e N (\dot{\theta}_{ir}^r - \omega_{iby}^b)) \\ & \quad + NT_{dm} + T_{dr} \\ & \quad + N(N-1)J_m \dot{\omega}_{iby}^b \\ & \quad - N^2 J_m \ddot{\theta}_{ir}^r \end{aligned} \quad (18)$$

$$\begin{aligned}
 J_{az}\ddot{\theta}_a &= -J_{az}\dot{\omega}_{ipz}^p \\
 &+ \frac{NK_t}{R_m} \left(u_a \right. \\
 &\left. - K_e N (\dot{\theta}_{ia}^a - \omega_{ibz}^a) \right) \\
 &+ (NT_{dm} + T_{da}) \\
 &+ N(N-1)J_m\omega_{ibz}^a \\
 &- N^2J_m\ddot{\theta}_{ia}^a
 \end{aligned} \tag{19}$$

2.3. Deriving the State Space Equations of the 3-DOF ISP Plant

Remark 1: According to the state space obtained in [8], it can be seen that this state space equation is not affine with respect to the angular velocity variable, and therefore it is not suitable for designing a nonlinear observer. To solve this problem, in the following, a new formulation of the state-space equation for 3-DOF ISP plant is obtained, which is affine with respect to the angular velocity.

According to the equations presented in (17)-(19), the nonlinear state space model for a 3-DOF ISP plant with assumptions that $x_1 = \theta_p, x_2 = \dot{\theta}_p, x_3 = \theta_r, x_4 = \dot{\theta}_r, x_5 = \theta_a, x_6 = \dot{\theta}_a, y_1 = \theta_p, y_2 = \theta_r$ and $y_3 = \theta_a$ can be modeled as follows:

$$\begin{cases} \dot{\theta} = \omega \\ \dot{\omega} = h(\theta) + H(\theta)\omega + B(\theta)u \end{cases} \tag{20}$$

where $\theta = [\theta_p \ \theta_r \ \theta_a]^T$ is the angular position vector and $\omega = [\dot{\theta}_p \ \dot{\theta}_r \ \dot{\theta}_a]^T$ is the angular velocity vector of the gimbal. In equation (20), the matrix $B(\theta)$ is a 3×3 diagonal matrix as follows:

$$B(\theta) = \begin{bmatrix} \frac{NK_t}{(J_{px} + J_{ax})R_m} & 0 & 0 \\ 0 & \frac{NK_t}{(J_{ry} + (J_{ay} + J_{py})\cos^2(\theta_p))R_m} & 0 \\ 0 & 0 & \frac{NK_t}{J_{az}R_m} \end{bmatrix} \tag{21}$$

Also, matrix $H(\theta)$ is a functional matrix whose elements include only boundary functions such as $\sin(\theta)$ and $\cos(\theta)$ and is defined as follows:

$$H(\theta) = \begin{bmatrix} 0 & H_{12}(\theta) & H_{13}(\theta) \\ H_{21}(\theta) & H_{22}(\theta) & H_{23}(\theta) \\ H_{31}(\theta) & H_{32}(\theta) & 0 \end{bmatrix} \tag{22}$$

Finally, vector $h(\theta)$ is also expressed as follows:

$$h(\theta) = [h_1(\theta) \ h_2(\theta) \ h_3(\theta)] \tag{23}$$

The elements of matrix $H(\theta)$ and vector $h(\theta)$ are introduced in Appendix.

In the state space equations obtained in (20), to improve the performance of the designed controller as well as reduce the implementation costs, it is assumed that the position vector θ is available and measurable and the angular velocity vector ω is unmeasurable which must be estimated.

3. PROPOSED OBSERVER-BASED CONTROL

The suggested observer for dealing with the nonlinear model (20), in addition to the ability to estimate the angular velocity with very high accuracy, should be designed in such a way that it is possible to design a simple and efficient controller for the observed system. For this purpose, a nonlinear observer-based state feedback controller will be designed. In the following, some preliminary Lemmas for designing the proposed controller strategy are provided.

3.1. Preliminaries

In this subsection, some preliminary Lemmas are presented.

Lemma 1 (A Lyapunov exponential stability theorem) [40]: The nonlinear system $\dot{x} = f(x)$ is exponentially stable, if there exists a continuously differentiable function $V(x)$ and positive constants ρ_1, ρ_2, ρ_3 , and τ such that

$$\begin{aligned}
 \rho_1 \|x\|^\tau &\leq V(x) \leq \rho_2 \|x\|^\tau \\
 \frac{\partial V}{\partial x} \cdot f(x) &\leq -\rho_3 \|x\|^\tau
 \end{aligned} \tag{24}$$

where $\|x\| = \sqrt{x^T x}$ is defined as the Euclidean norm.

Proof: see [40].

Lemma 2: For any variables $\alpha, \beta \in \mathbb{R}^n$ the inequality (25) is always established:

$$\alpha^T \beta \leq \frac{1}{2} \|\alpha\|^2 + \frac{1}{2} \|\beta\|^2 \tag{25}$$

Proof:

$$\begin{aligned}
 \|\alpha - \beta\|^2 \geq 0 &\rightarrow \|\alpha\|^2 + \|\beta\|^2 - 2\alpha^T \beta \geq 0 \\
 &\rightarrow \alpha^T \beta \leq \frac{1}{2} \|\alpha\|^2 + \frac{1}{2} \|\beta\|^2
 \end{aligned} \tag{26}$$

Lemma 3: For any bounded matrix function $A(\theta) \in \mathbb{R}^{n \times n}$, the following inequalities always hold:

$$\|A(\theta)\| \leq \frac{1}{2} \gamma_1, \quad \gamma_1 > 1 \tag{27}$$

$$A(\theta) + A^T(\theta) \leq \frac{1}{2} \gamma_2 I, \quad \gamma_2 > 1 \tag{28}$$

where $\|A\| = \sqrt{\lambda_{\max}(A^T A)} = \sigma_{\max}(A)$ is defined as the spectral norm of a matrix A and $\sigma_{\max}(\cdot)$ represents the largest singular value of matrix A [41].

Proof:

a)

$$\begin{aligned}
 \|A(\theta)\| &= \sqrt{\lambda_{\max}(A^T(\theta)A(\theta))} = \sigma_{\max}(A(\theta)) \\
 &\leq \left(\sum_{i=1}^n \sum_{j=1}^n |a_{ij}|^2 \right)^{\frac{1}{2}} = \left(\sum_{k=1}^n \sigma_k \right)^{\frac{1}{2}}
 \end{aligned}$$

Therefore, $\gamma_1 = 2 * \sup(\sum_{k=1}^n \sigma_k)^{\frac{1}{2}}$, where σ_k represents the singular value of matrix A .

b)

$$A(\theta) + A^T(\theta) \leq |\lambda_{\max}\{A(\theta) + A^T(\theta)\}| I$$

Therefore, $\gamma_2 = 2 * \sup(|\lambda_{max}\{A(\theta) + A^T(\theta)\}|)$, where $\lambda_{max}(\cdot)$ represents the eigen value of matrix $A + A^T$.

3.2. Nonlinear Observer Design

In the first step, to design an observer for the 3-DIF ISP plant, we need to simplify equations (20). As can be seen, all elements on the main diagonal of the matrix $B(\theta)$ in equation (23) are always positive constants that depend on the parameters of the ISP system. This means that the $B(\theta)$ is always a non-singular and invertible matrix. Next, to eliminate the nonlinear term $h(\theta)$, the input vector u is considered as follows:

$$u = B^{-1}(\theta)(-h(\theta) + v) \tag{29}$$

In equation (29), the vector v is defined as the new input of the system, which will be determined in the following design steps. By substituting the control signal (29) in the system state space equation (20), one has:

$$\begin{cases} \dot{\theta} = \omega \\ \dot{\omega} = H(\theta)\omega + v \end{cases} \tag{30}$$

As mentioned, it is assumed that the position vector θ is available and measurable but the angular velocity vector ω is not available and must be estimated. Hence, there is a need for an observer who can estimate the internal states of the system. Assume that $\hat{\theta}$ and $\hat{\omega}$ are the estimated values of the internal states of the system. Then, the observer equations can be considered as follows:

$$\begin{cases} \dot{\hat{\theta}} = k_1\tilde{\theta} + \hat{\omega} \\ \dot{\hat{\omega}} = k_2\tilde{\theta} + H(\theta)\hat{\omega} + v \end{cases} \tag{31}$$

Note that the above estimation rules are applicable because only the available variables ($\hat{\omega}$, $\hat{\theta}$ and θ) are used and the non-measurable variable ω is not used. Also, the parameters k_1 and k_2 are constant coefficients that are determined according to the suggested Lyapunov function in the next steps. By definition $\tilde{\theta} = \theta - \hat{\theta}$ and $\tilde{\omega} = \omega - \hat{\omega}$ as the estimated system state error, one has:

$$\begin{aligned} \dot{\tilde{\theta}} &= \{\dot{\theta} - \dot{\hat{\theta}}\} = \{(\omega) - (k_1\tilde{\theta} + \hat{\omega})\} \\ &= -k_1\tilde{\theta} + (\omega - \hat{\omega}) \\ &= -k_1\tilde{\theta} + \tilde{\omega} \\ \dot{\tilde{\omega}} &= \{\dot{\omega} - \dot{\hat{\omega}}\} = (H(\theta)\omega + v) \\ &\quad - (k_2\tilde{\theta} + H(\theta)\hat{\omega} + v) \\ &= -k_2\tilde{\theta} + H(\theta)(\omega - \hat{\omega}) \\ &= -k_2\tilde{\theta} + H(\theta)\tilde{\omega} \end{aligned} \tag{32}$$

Consider the following Lyapunov candidate:

$$V_o = \begin{bmatrix} \tilde{\theta}^T & \tilde{\omega}^T \end{bmatrix} \begin{bmatrix} \gamma^2 & -\frac{1}{2}\gamma \\ -\frac{1}{2}\gamma & \frac{2}{3} \end{bmatrix} \begin{bmatrix} \tilde{\theta} \\ \tilde{\omega} \end{bmatrix} \tag{33}$$

$$= \gamma^2\tilde{\theta}^T\tilde{\theta} - \gamma\tilde{\theta}^T\tilde{\omega} + \frac{2}{3}\tilde{\omega}^T\tilde{\omega}, \quad \gamma = \max\{\gamma_1, \gamma_2\}$$

In matrix function (33), $\gamma > 1$, so $\begin{bmatrix} \gamma^2 & -\frac{1}{2}\gamma \\ -\frac{1}{2}\gamma & \frac{2}{3} \end{bmatrix} > 0$ and therefore, the Lyapunov function (33) is positive definite.

The time derivative of the Lyapunov function V_o is obtained by:

$$\dot{V}_o = 2\gamma^2\tilde{\theta}^T\dot{\tilde{\theta}} - \gamma\tilde{\theta}^T\dot{\tilde{\omega}} - \gamma\tilde{\omega}^T\dot{\tilde{\theta}} + \frac{4}{3}\tilde{\omega}^T\dot{\tilde{\omega}} \tag{34}$$

By considering the equation of the estimated system state error (32), the time derivative of the Lyapunov function (33) equals to:

$$\begin{aligned} \dot{V}_o &= 2\gamma^2\tilde{\theta}^T(-k_1\tilde{\theta} + \tilde{\omega}) \\ &\quad - \gamma\tilde{\theta}^T(-k_2\tilde{\theta} + H(\theta)\tilde{\omega}) \\ &\quad - \gamma\tilde{\omega}^T(-k_1\tilde{\theta} + \tilde{\omega}) \\ &\quad + \frac{4}{3}\tilde{\omega}^T(-k_2\tilde{\theta} + H(\theta)\tilde{\omega}) \\ &= (-2\gamma^2k_1 + \gamma k_2)\tilde{\theta}^T\tilde{\theta} \\ &\quad + \left(2\gamma^2 + k_1\gamma - \frac{4}{3}k_2\right)\tilde{\theta}^T\tilde{\omega} \\ &\quad - \gamma\tilde{\theta}^TH(\theta)\tilde{\omega} + \tilde{\omega}^T(-\gamma I \\ &\quad + \frac{4}{3}H(\theta))\tilde{\omega} \end{aligned} \tag{35}$$

To cancel the cross-product terms, we choose:

$$2\gamma^2 + k_1\gamma - \frac{4}{3}k_2 = 0 \rightarrow \begin{cases} k_1 = 2\gamma \\ k_2 = 3\gamma^2 \end{cases} \tag{36}$$

Therefore, substituting (36) in (35) leads

$$\begin{aligned} \dot{V}_o &= -\gamma^3\|\tilde{\theta}\|^2 - \gamma\tilde{\theta}^TH(\theta)\tilde{\omega} \\ &\quad + \tilde{\omega}^T(-\gamma I \\ &\quad + \frac{2}{3}(H(\theta) + H^T(\theta)))\tilde{\omega} \end{aligned} \tag{37}$$

According to Lemma 3:

$$\begin{aligned} |\gamma\tilde{\theta}^TH(\theta)\tilde{\omega}| &\leq \gamma\|\tilde{\theta}\|\|\tilde{\omega}\|\|H(\theta)\| \\ &\stackrel{\|H(\theta)\| \leq \frac{1}{2}\gamma}{\implies} |\gamma\tilde{\theta}^TH(\theta)\tilde{\omega}| \\ &\leq \frac{1}{2}\gamma^2\|\tilde{\theta}\|\|\tilde{\omega}\| \end{aligned} \tag{38}$$

Then with the help of Lemma 2:

$$\begin{aligned} \frac{1}{2}\gamma^2\|\tilde{\theta}\|\|\tilde{\omega}\| &= \frac{1}{2}\left(\gamma^{\frac{3}{2}}\|\tilde{\theta}\|\right)\left(\gamma^{\frac{1}{2}}\|\tilde{\omega}\|\right) \\ &\leq \frac{1}{4}\gamma^3\|\tilde{\theta}\|^2 + \frac{1}{4}\gamma\|\tilde{\omega}\|^2 \end{aligned} \tag{39}$$

substituting (28) and (39) in (37) yields:

$$\begin{aligned} \dot{V}_o &\leq -\frac{3}{4}\gamma^3\|\tilde{\theta}\|^2 - \frac{5}{12}\gamma\|\tilde{\omega}\|^2 \\ &\leq -\frac{\gamma}{3}(\|\tilde{\theta}\|^2 + \|\tilde{\omega}\|^2) \end{aligned} \tag{40}$$

The following theorem expresses the convergence of the designed observer.

Theorem 1: By designing the dynamics of the observer for system (30) in the form of equation (31), the angular

velocity vector is estimated with very good accuracy, and the observed system (32) is exponential stable.

Proof: To prove the exponentially stability of the observed system, the selected Lyapunov function must satisfy the Lemma 1 conditions. The upper and lower bounds of the suggested Lyapunov function (33) are obtained using Lemma 2 as follows:

$$\gamma \tilde{\theta}^T \tilde{\omega} \leq \frac{1}{2} \gamma^2 \tilde{\theta}^T \tilde{\theta} + \frac{1}{2} \tilde{\omega}^T \tilde{\omega} \rightarrow -\gamma \tilde{\theta}^T \tilde{\omega} \geq -\frac{1}{2} \gamma^2 \tilde{\theta}^T \tilde{\theta} - \frac{1}{2} \tilde{\omega}^T \tilde{\omega} \quad (41)$$

Therefore, the lower bound of the Lyapunov function (33) is obtained as follows:

$$\begin{aligned} V_o &= \gamma^2 \tilde{\theta}^T \tilde{\theta} - \gamma \tilde{\theta}^T \tilde{\omega} + \frac{2}{3} \tilde{\omega}^T \tilde{\omega} \\ &\geq \left(\gamma^2 \tilde{\theta}^T \tilde{\theta} - \frac{1}{2} \gamma^2 \tilde{\theta}^T \tilde{\theta} \right) \\ &\quad + \left(-\frac{1}{2} \tilde{\omega}^T \tilde{\omega} + \frac{2}{3} \tilde{\omega}^T \tilde{\omega} \right) \\ &= \frac{1}{2} \gamma^2 \|\tilde{\theta}\|^2 + \frac{1}{6} \|\tilde{\omega}\|^2 \\ &\geq \frac{1}{6} (\|\tilde{\theta}\|^2 + \|\tilde{\omega}\|^2) \end{aligned} \quad (42)$$

Considering (41), the upper band of the Lyapunov function (33) is as follows:

$$\begin{aligned} V_o &= \gamma^2 \tilde{\theta}^T \tilde{\theta} - \gamma \tilde{\theta}^T \tilde{\omega} + \frac{2}{3} \tilde{\omega}^T \tilde{\omega} \\ &\leq \left(\gamma^2 \tilde{\theta}^T \tilde{\theta} + \frac{1}{2} \gamma^2 \tilde{\theta}^T \tilde{\theta} \right) + \left(\frac{1}{2} \tilde{\omega}^T \tilde{\omega} + \frac{2}{3} \tilde{\omega}^T \tilde{\omega} \right) \\ &= \frac{3}{2} \gamma^2 \|\tilde{\theta}\|^2 + \frac{7}{6} \|\tilde{\omega}\|^2 \\ &\leq 2\gamma^2 (\|\tilde{\theta}\|^2 + \|\tilde{\omega}\|^2) \end{aligned} \quad (43)$$

So

$$\begin{aligned} \frac{1}{6} (\|\tilde{\theta}\|^2 + \|\tilde{\omega}\|^2) &\leq V_o \\ &\leq 2\gamma^2 (\|\tilde{\theta}\|^2 + \|\tilde{\omega}\|^2) \end{aligned} \quad (44)$$

Therefore, the first condition of Lemma 1 is established in such a way that $\rho_1 = \frac{1}{6}$ and $\rho_2 = 2\gamma^2$. It is also clear from relation (40) that the second condition hold and $\rho_3 = \frac{\gamma}{3}$. By combining inequalities (40) and (43), one has:

$$\begin{aligned} \dot{V}_o(t) &\leq -\frac{\gamma}{3} (\|\tilde{\theta}\|^2 + \|\tilde{\omega}\|^2) \leq -\frac{\gamma}{3} * \frac{1}{2\gamma^2} V_o \\ &\rightarrow \dot{V}_o(t) \leq -\frac{1}{6\gamma} V_o(t) \\ &\rightarrow V_o(t) \leq e^{-\frac{t}{6\gamma}} V_o(0) \end{aligned} \quad (45)$$

So

$$\begin{aligned} (\|\tilde{\theta}(t)\|^2 + \|\tilde{\omega}(t)\|^2) &\leq 12\gamma^2 e^{-\frac{t}{6\gamma}} (\|\tilde{\theta}(0)\|^2 + \|\tilde{\omega}(0)\|^2) \end{aligned} \quad (46)$$

Inequality (46) clearly shows the convergence of estimation error (32), i.e.:

$$\begin{aligned} \|\tilde{\theta}(t)\| \rightarrow 0 &\xrightarrow{\tilde{\theta}=\theta-\hat{\theta}} \hat{\theta} \rightarrow \theta \\ \|\tilde{\omega}(t)\| \rightarrow 0 &\xrightarrow{\tilde{\omega}=\omega-\hat{\omega}} \hat{\omega} \rightarrow \omega \end{aligned} \quad (47)$$

Therefore, the proof of Theorem 1 is completed. ■

3.3. Control Strategy Design

In this section, the desired controller is designed for the system (31). For this purpose, the term v can be considered as a virtual control signal in the form of equation (48):

$$v = -(3\gamma^2 \tilde{\theta} + H(\theta) \hat{\omega}) + k \quad (48)$$

substituting (48) in (31) results in:

$$\begin{cases} \dot{\hat{\theta}} = 2\gamma \tilde{\theta} + \hat{\omega} \\ \dot{\hat{\omega}} = 3\gamma^2 \tilde{\theta} + H(\theta) \hat{\omega} + \{-(3\gamma^2 \tilde{\theta} + H(\theta) \hat{\omega}) + k\} \\ \quad \quad \quad = k \end{cases} \quad (49)$$

Since it has been proved that $\tilde{\theta}$ tends to zero, therefore, (49) is simplified as follows:

$$\begin{cases} \dot{\hat{\theta}} = \hat{\omega} \\ \dot{\hat{\omega}} = k \end{cases} \quad (50)$$

By considering the virtual control signal k as state feedback, the equations of state of the closed-loop system (50) are transformed as follows:

$$\begin{cases} \dot{\hat{\theta}} = \hat{\omega} \\ \dot{\hat{\omega}} = -c_1 \hat{\theta} - c_2 \hat{\omega} \end{cases} \quad (51)$$

The above closed-loop system is a simple linear form that can be controlled by conventional control approaches such as the pole placement method. The overall observer-based control structure is demonstrated in Fig. 3.

Finally, the proposed algorithm for designing an observer-based control method for 3-DOF ISP systems is summarized in Fig. 4.

4. SIMULATION RESULTS

This section is devoted to simulating the 3-DOF ISP system presented in Fig. 1. The proposed observer-based control method is used to control the 3-DOF ISP plant (20) with parameter information provided in Table 1 [8].

Remark 2: Since the control performance of the 3-DOF ISP plant is strongly affected by wind disturbance, mass imbalance torque, and friction torque, a set of friction torque and mass imbalance torque is simulated to evaluate the effectiveness of the suggestion control approach.

To simulate the wind disturbance and consider the mass imbalance torque, T_{dl} is represented by a bounded random function as follows [25]:

$$T_{dl}(t) = 2.034(rand(t) - 0.5), l = p, r, a \quad (52)$$

Since the Friction torque is a major part of T_{dm} , therefore, a sinusoidal function is suggested to represent the disturbance torque imposed on the ISP as following equation [25]:

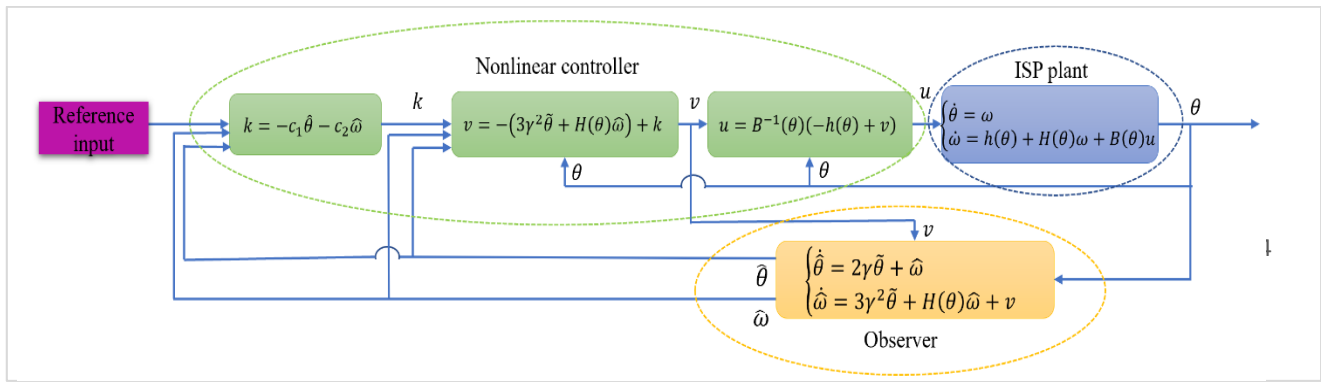


Fig. 3: Structure of the observer-based control strategy.

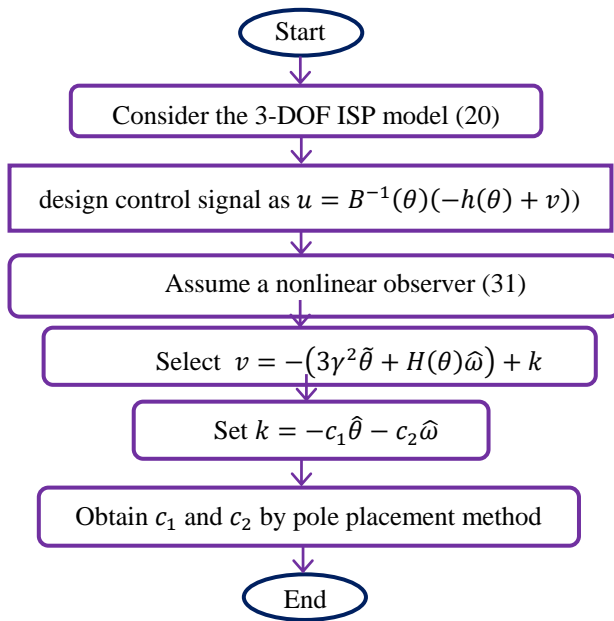


Fig. 4: The algorithm for designing observer-based control method for 3-DOF ISP system.

Table 1: Parameters of an ISP plant.

Parameter	Definition	Value
R_m	Armature resistance	7.56 Ω
K_t	Motor torque constant	0.127 Nm/Amp
K_e	Back EMF constant	0.128 V/rad/s
N	Drive ratio	104.7
J_L	Payload inertial	2.2 Kg m^2
J_m	Motor inertial	1.8006e-5 Kg m^2

$$T_{dm} = 0.06(\sin(t/5) + \sin(t/10)) \quad (53)$$

Also, to evaluate the robustness of the suggestion control strategy against the model uncertainties, 9 uncertain parameters have been added as shown in Table 2.

To evaluate the performance of the suggested observer-based control method, two simulation scenarios are considered. In the first scenario, only the ability to stabilize the proposed control is examined. In the second one, a different profile is considered for the roll, pitch, and yaw gimbal angle, and the controller's ability to track different outputs is evaluated.

Table 2: Variation Range of the moments of inertia [25].

J_p	J_a	J_r
$J_{px} = 0.769 + 0.307 * rand(t) - 0.$	$J_{ax} = 0.975 + 0.390 * rand(t) - 0.$	$J_{rx} = 1.048 + 0.419 * rand(t) - 0.$
$J_{py} = 0.925 + 0.381 * rand(t) - 0.$	$J_{ay} = 2.546 + 1.018 * rand(t) - 0.$	$J_{ry} = 2.763 + 1.105 * rand(t) - 0.$
$J_{pz} = 1.016 + 0.406 * rand(t) - 0.$	$J_{az} = 2.732 + 1.093 * rand(t) - 0.$	$J_{rz} = 2.984 + 1.194 * rand(t) - 0.$

4.1. Scenario 1 (Stabilization Results)

In this scenario, the steady-state equations of the 3-DOF ISP model (20), dynamics of the nonlinear observer (31), and the dynamics of the state feedback control system (49) have been simulated in MATLAB and the details of the stabilization control responses obtained by applying the proposed observer-based controller are provided in Figs. 5-8.

Figs. 5a and 5b show the pitch positions θ_p , and pitch velocities $\dot{\theta}_p$. As can be seen in Figs. 5a and 5b, the θ_p and $\dot{\theta}_p$ are stabilized by the designed controller and converge to zero in about 0.5 seconds. Figs. 6a and 6b shows that the performance of the proposed controller is in the acceptable range and it can stabilize roll positions θ_r and roll velocities $\dot{\theta}_r$, in less than 0.5 seconds. Figs. 7a and 7b illustrates that the stabilization time for regulated θ_a and $\dot{\theta}_a$ is about 0.45 seconds. Finally, Figs. 8a-8c shows the smooth control input signals u_p , u_r , and u_a , respectively. Based on these figures, it is clear that the designed observer has a very good performance and can accurately estimate the speed and position of each roll, pitch, and yaw gimbal angle in a short time.

4.2. Scenario 2 (Tracking Results)

To demonstrate the effectiveness and proper performance of the proposed controller strategy, the case of tracking desired references has been examined. In the following, we consider a different profile for each of the gimbal angles and examine the performance of the proposed controller.

4.2.1. Pitch position

It is assumed that the desired reference of the pitch angle is per with the following profile:

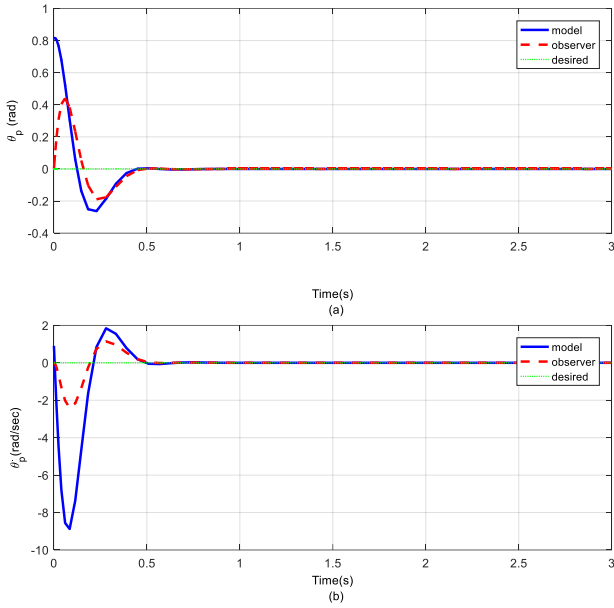


Fig. 5: State response of close-loop 3-DOF ISP system for scenario 1, (a) The pitch positions (θ_p), (b) The pitch velocities ($\dot{\theta}_p$).

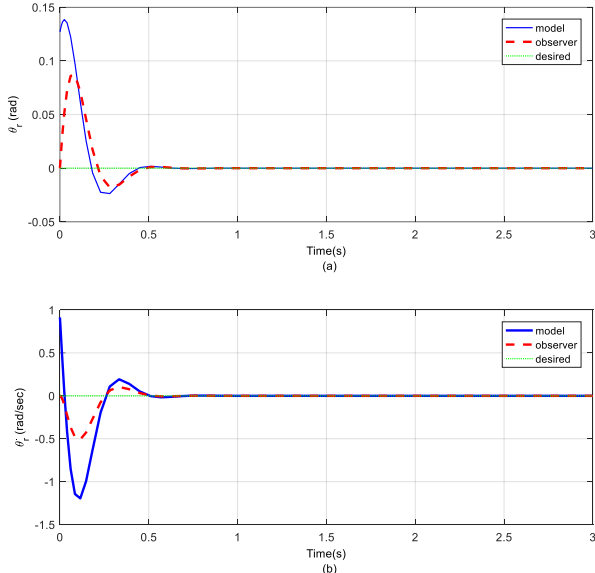


Fig. 6: State response of close-loop 3-DOF ISP system for scenario 1, (a) The roll positions (θ_r), (b) The roll velocities ($\dot{\theta}_r$).

$$\begin{cases} 1 & 1 \leq t < 5 \\ 1.5 & 5 \leq t < 10 \\ 1 & 10 \leq t < 15 \\ 0.1 * \sin(t) & 15 \leq t < 30 \end{cases} \quad (54)$$

By applying the proposed controller, the closed-loop pitch position and pitch velocities to track the reference input (54) for the observer and the model is shown in Fig. 9.

4.2.2. Roll position

The desired input to track roll angle is assumed to be as follows:

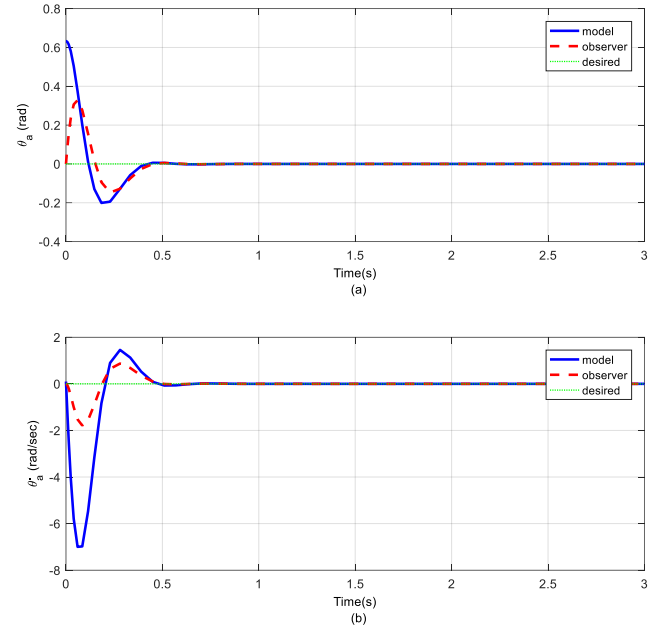


Fig. 7: State response of close-loop 3-DOF ISP system for scenario 1, (a): The yaw positions (θ_a), (b): The yaw velocities ($\dot{\theta}_a$).

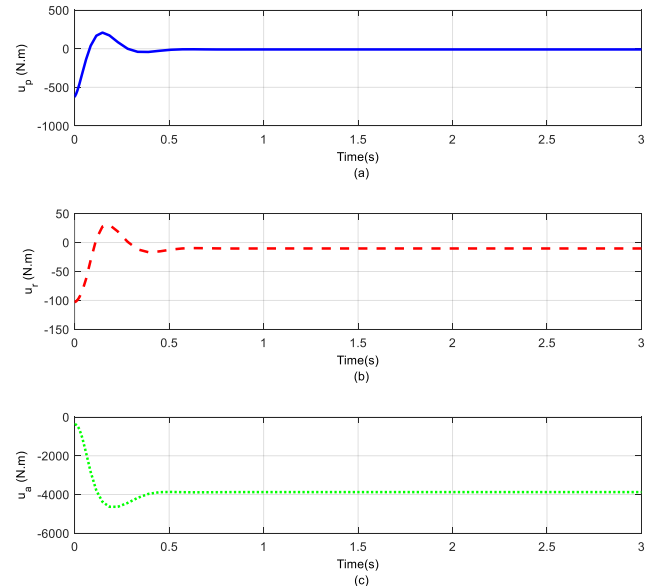


Fig. 8: Control signal of close-loop 3-DOF ISP system for scenario 1, (a) u_p , (b) u_r , (c) u_a .

$$\begin{cases} -2 & 1 \leq t < 5 \\ -1.5 & 5 \leq t < 10 \\ -1 & 10 \leq t < 15 \\ 0.1 * \sin(t) & 15 \leq t < 30 \end{cases} \quad (55)$$

How to track the profile (55) for the roll angle state is also illustrated in Fig. 10.

4.2.3. Yaw position

For the yaw angular variable, the desired input is considered as profile (56):

$$\begin{cases} 3 & 1 \leq t < 5 \\ 2.5 & 5 \leq t < 10 \\ 2 & 10 \leq t < 15 \\ 0.1 * \sin(t) & 15 \leq t < 30 \end{cases} \quad (56)$$

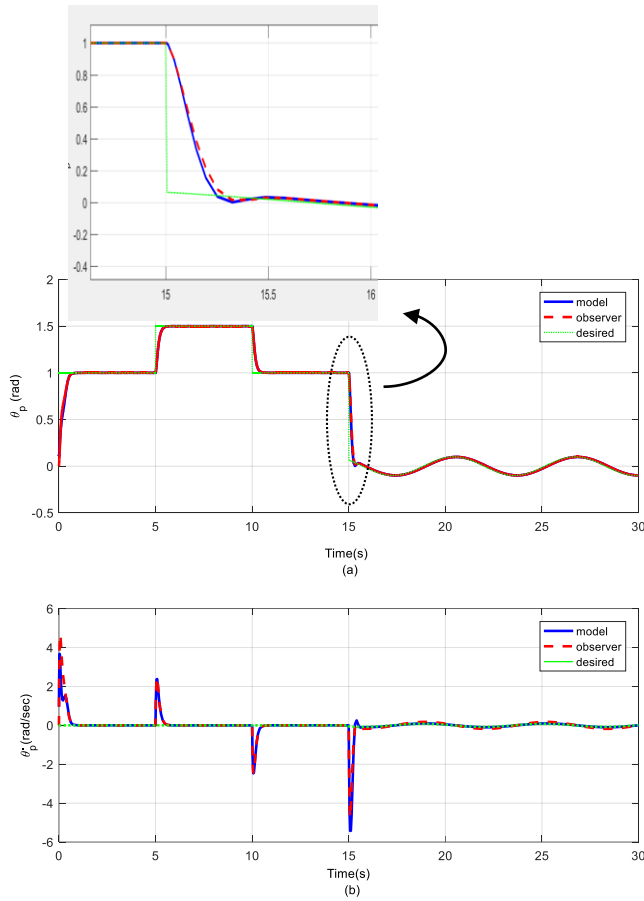


Fig. 9: State response of close-loop 3-DOF ISP system for scenario 2, (a) The pitch positions (θ_p), (b) The pitch velocities ($\dot{\theta}_p$).

The variations of the yaw angular variable to follow the above path are shown in Fig. 11.

Figs. 9-11 reveal that the angular positions of pitch, roll and yaw are well-tracked by the proposed control strategy. As can be seen, the closed-loop system is well able to follow the assumed paths for all three system states, and the amount of tracking error is acceptable. Finally, Fig. 12 shows the control efforts u_p , u_r , and u_a for Scenario 2.

Remark 3: It is important to mention that in most of the methods proposed to control the position of the ISP system in the current literature, it has been assumed that all required states with appropriate accuracy are available. In this paper, to reduce the number of measuring devices and also to increase the accuracy of the angular velocity value, instead of expensive gyroscopes, a velocity observer has been used. Also, in theorem 1, it was proved that the error of the designed nonlinear observer exponentially tends to zero and this allows us to estimate the angular velocity with very good accuracy. Given the above, comparing the observer-based control method proposed in this paper with previous methods is not fair because the performance of the output feedback controller at its best is the same performance as the state feedback controller when all system variables are available. To evaluate the performance and quality of the suggested observer algorithm, the following two performance indexes are utilized.

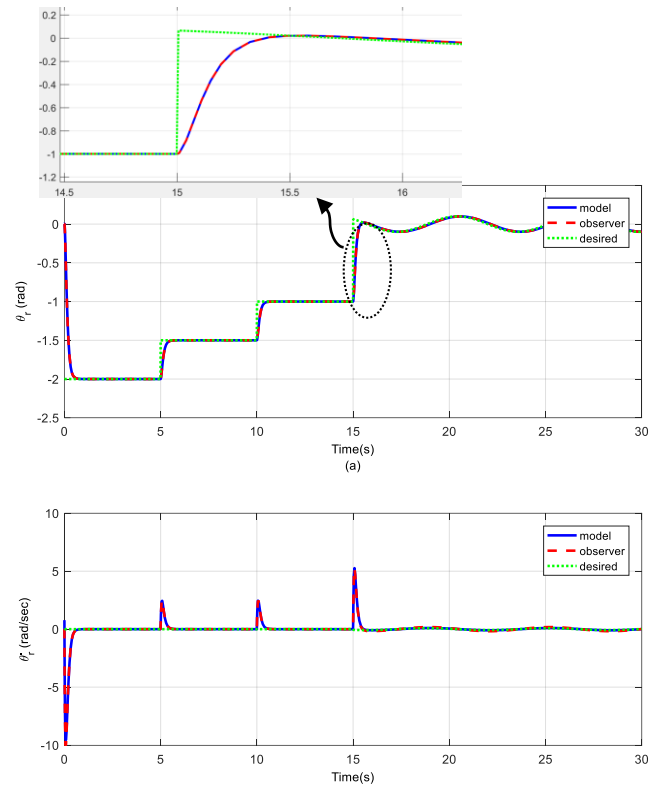


Fig. 10: State response of close-loop 3-DOF ISP system for scenario 2, (a) The roll positions (θ_r), (b) The roll velocities ($\dot{\theta}_r$).

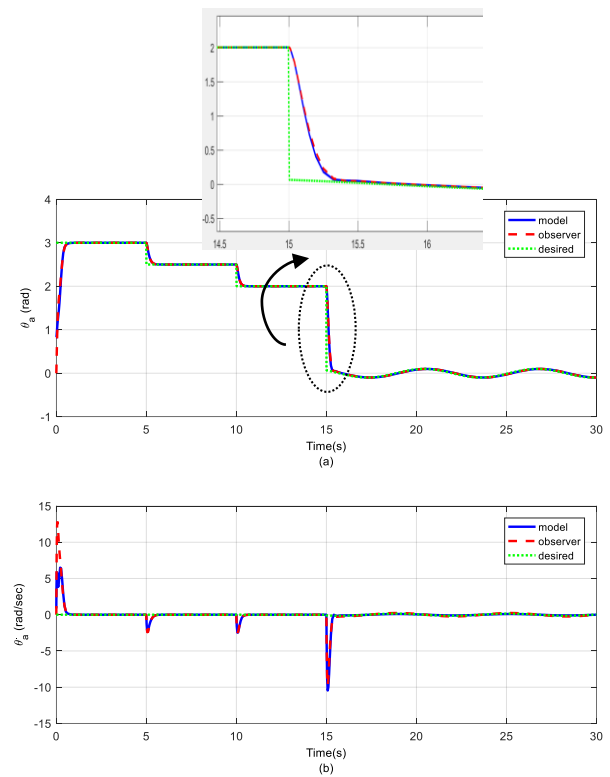


Fig. 11: State response of close-loop 3-DOF ISP system for scenario 2, (a) The yaw positions (θ_a), (b) The yaw velocities ($\dot{\theta}_a$).

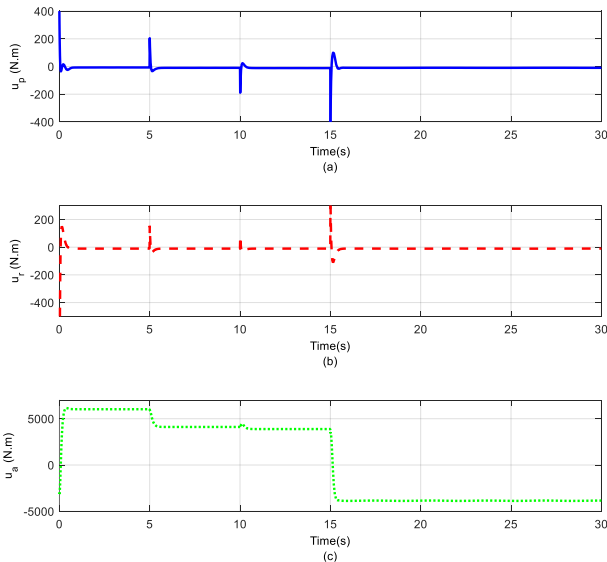


Fig. 12: Control signal of close-loop 3-DOF ISP system for scenario 2, (a) u_p , (b) u_r , (c) u_a .

4.2.4. The Integral Square Error (ISE) performance index

ISE is one of the indexes used to show the level of deviation of tracking errors in control systems and is defined as follows:

$$ISE = \int_0^{t_s} (y_{obs}(t) - y_{sys}(t))^2 dt \quad (57)$$

where $y_{obs}(t)$ and y_{sys} are defined as the observer output and system output respectively, and t_s represents the simulation time.

4.2.5. The Maximum Absolute Value (MAV) performance index

MAV criterion is used to evaluate the tracking accuracy, which is defined as formula (58):

$$MAV = \max_{t \in [0, t_s]} |y_{obs}(t) - y_{sys}(t)| \quad (58)$$

The browser performance for all variables in both scenarios is summarized in Table 3. Based on this table, it can be seen that the designed observer has a satisfactory performance and has been able to estimate the system variables with good accuracy.

Remark 4: Compared to other existing control strategies, the superiority of the strategy proposed in this paper is in cases such as:

- 1- Reducing the cost of construction and reducing the weight of the control system connected to the moving object through the removal of expensive gyroscopes
- 2- Easy implementation, and its efficiency.

3- CONCLUSION

This paper suggested the issue of observer-based control of the 3-DOF ISP system. To control ISP systems, in addition to measuring the angular position, angular velocity is also

Table 3: Parameter’s performance indexes for two scenarios.

Index	State variable	Value	
		Scenario 1	Scenario 2
ISE	pitch positions (θ_p)	0.0005	0.0018
	pitch velocities ($\dot{\theta}_p$)	0.0877	0.8458
	roll positions (θ_r)	0.0236	6.34e-5
	roll velocities ($\dot{\theta}_r$)	3.0731	0.0862
	yaw positions (θ_a)	0.0084	0.0210
	yaw velocities ($\dot{\theta}_a$)	1.1840	3.277
MAV	pitch positions (θ_p)	0.1190	0.1067
	pitch velocities ($\dot{\theta}_p$)	0.8483	1.4782
	roll positions (θ_r)	0.8436	0.0242
	roll velocities ($\dot{\theta}_r$)	6.2314	0.4230
	yaw positions (θ_a)	0.4053	0.7324
	yaw velocities ($\dot{\theta}_a$)	3.7367	6.304

required. Gyroscopes used to accurately measure angular velocity are expensive and also always have error measurement values due to gyroscope drift. On the other hand, there are limitations on the weight and volume of stabilization systems, therefore if angular velocity can be measured accurately and at the lowest possible cost, it is possible to achieve high performance and more economically in practical design. To reduce the expressed problems, the velocity observer is used to estimate the velocity vector based on the Lyapunov theorem. For this purpose, first, to design an efficient observer, the state space equation for the ISP system is rewritten to a new form. Then with the help of the Lyapunov-based nonlinear control technique, a nonlinear observer is designed to improve the velocity estimation of the ISP plant. Finally, through Theorem 1, the exponential stability and convergence of the observer system are proved. The simulation results showed that the proposed control method is efficient and can track different sources well. In future work, we can suggest some implementation issues that may come up in experimental settings, such as constraints on system state variables, state time delay, or input saturation for designing the high-performance ISP controller.

APPENDIX

Based on equations (17) - (19), the elements of the $H(\theta)$ and $h(\theta)$ are obtained as follows:

$$\begin{aligned}
 H_{12}(\theta) = & \omega_{ibz}^b * \cos(\theta_r) + \omega_{ibx}^b * \sin(\theta_r) \\
 & + (\sin(\theta_p) * (\sin(\theta_p) * (\omega_{ibz}^b \\
 & * \cos(\theta_r) - \omega_{ibx}^b * \sin(\theta_r)) \\
 & + \omega_{iby}^b * \cos(\theta_p)) * (J_{ay} - J_{az} \\
 & + J_{py} - J_{pz}) / (J_{ax} + J_{px}) \\
 & - (\cos(\theta_p) * (\cos(\theta_p) * (\omega_{ibz}^b \\
 & * \cos(\theta_r) - \omega_{ibx}^b * \sin(\theta_r)) \\
 & - \omega_{iby}^b * \sin(\theta_p)) * (J_{ay} - J_{az} \\
 & + J_{py} - J_{pz}) / (J_{ax} + J_{px})
 \end{aligned}$$

$$\begin{aligned}
 H_{13}(\theta) = & (J_{az} * (\sin(\theta_p) * (\omega_{ibz}^b * \cos(\theta_r) - \omega_{ibx}^b \\
 & * \sin(\theta_r)) + \omega_{iby}^b \\
 & * \cos(\theta_p)) / (J_{ax} + J_{px})
 \end{aligned}$$

$$\begin{aligned}
 H_{21}(\theta) = & -J_{ax} * \omega_{ibx}^b * \sin(\theta_r) + J_{px} * \omega_{ibx}^b \\
 & * \sin(\theta_r) - J_{ax} * \omega_{ibz}^b * \cos(\theta_r) \\
 & - J_{px} * \omega_{ibz}^b * \cos(\theta_r) / (J_{ry} + J_{ay}) \\
 & * \cos^2(\theta_p) + J_{py} * \cos^2(\theta_p)
 \end{aligned}$$

$$\begin{aligned}
 H_{22}(\theta) = & (J_{ay} * \cos^2(\theta_p) + J_{py} * \cos^2(\theta_p) + J_{az} \\
 & * \sin^2(\theta_p) + J_{pz} * \sin^2(\theta_p) - J_{ay} \\
 & * \omega_{ibx}^b * \cos(\theta_p) * \cos(\theta_r) \\
 & * \sin(\theta_p) + J_{az} * \omega_{ibx}^b * \cos(\theta_p) \\
 & * \cos(\theta_r) * \sin(\theta_p) - J_{py} * \omega_{ibx}^b \\
 & * \cos(\theta_p) * \cos(\theta_r) * \sin(\theta_p) \\
 & + J_{pz} * \omega_{ibx}^b * \cos(\theta_p) * \cos(\theta_r) \\
 & * \sin(\theta_p) - J_{ay} * \omega_{ibz}^b * \cos(\theta_p) \\
 & * \sin(\theta_p) * \sin(\theta_r) + J_{az} * \omega_{ibz}^b \\
 & * \cos(\theta_p) * \sin(\theta_p) * \sin(\theta_r) \\
 & - J_{py} * \omega_{ibz}^b * \cos(\theta_p) * \sin(\theta_p) \\
 & * \sin(\theta_r) + J_{pz} * \omega_{ibz}^b * \cos(\theta_p) \\
 & * \sin(\theta_p) * \sin(\theta_r)) / (J_{ry} + J_{ay}) \\
 & * \cos^2(\theta_p) + J_{py} * \cos^2(\theta_p)
 \end{aligned}$$

(59)

$$\begin{aligned}
 H_{23}(\theta) = & -J_{az} * \sin(\theta_p) + J_{az} * \omega_{ibx}^b * \cos(\theta_p) \\
 & * \cos(\theta_r) + J_{az} * \omega_{ibz}^b * \cos(\theta_p) \\
 & * \sin(\theta_r)) / (J_{ry} + J_{ay} * \cos^2(\theta_p) \\
 & + J_{py} * \cos^2(\theta_p))
 \end{aligned}$$

$$\begin{aligned}
 H_{31}(\theta) = & \omega_{iby}^b * \cos(\theta_p) + \omega_{ibz}^b * \cos(\theta_r) * \sin(\theta_p) \\
 & - \omega_{ibx}^b * \sin(\theta_p) * \sin(\theta_r)
 \end{aligned}$$

$$\begin{aligned}
 H_{32}(\theta) = & \omega_{ibz}^b * \cos(\theta_p) * \sin(\theta_r) - \omega_{ibx}^b * \cos(\theta_p) \\
 & * \cos(\theta_r)
 \end{aligned}$$

And

$$\begin{aligned}
 h_1(\theta) = & (T_{dp} + N * T_{dm}) / (J_{ax} + J_{px}) - \dot{\omega}_{ibx}^b \\
 & * \cos(\theta_r) - \dot{\omega}_{ibz}^b * \sin(\theta_r) \\
 & - ((\sin(\theta_p) * (\omega_{ibz}^b * \cos(\theta_r) \\
 & - \omega_{ibx}^b * \sin(\theta_r)) + \omega_{iby}^b \\
 & * \cos(\theta_p)) * (\cos(\theta_p) * (\omega_{ibz}^b \\
 & * \cos(\theta_r) - \omega_{ibx}^b * \sin(\theta_r)) \\
 & - \omega_{iby}^b * \sin(\theta_p)) * (J_{ay} - J_{az} \\
 & + J_{py} - J_{pz}) / (J_{ax} + J_{px}) \\
 & + (J_m * N * (N - 1) * (\dot{\omega}_{ibx}^b \\
 & * \cos(\theta_r) - \dot{\omega}_{ibz}^b \\
 & * \sin(\theta_r))) / (J_{ax} + J_{px}) + (K_e \\
 & * K_t * N^2 * (\omega_{ibx}^b * \cos(\theta_r) \\
 & - \omega_{ibz}^b * \sin(\theta_r))) / (R_m * (J_{ax} \\
 & + J_{px}))
 \end{aligned}$$

$$\begin{aligned}
 h_3(\theta) = & \dot{\omega}_{iby}^b * \sin(\theta_p) - \cos(\theta_p) * (\dot{\omega}_{ibz}^b \\
 & * \cos(\theta_r) - \dot{\omega}_{ibx}^b * \sin(\theta_r)) \\
 & + (T_{da} + N * T_{dm}) / J_{az} + (J_m \\
 & * N * (N - 1) * (\omega_{ibz}^b * \cos(\theta_p) \\
 & * \cos(\theta_r) - \omega_{iby}^b * \sin(\theta_p) \\
 & + \omega_{ibx}^b * \cos(\theta_p) \\
 & * \sin(\theta_r))) / J_{az} + (K_e * K_t * N^2 \\
 & * (\omega_{ibz}^b * \cos(\theta_p) * \cos(\theta_r) \\
 & - \omega_{iby}^b * \sin(\theta_p) + \omega_{ibx}^b \\
 & * \cos(\theta_p) * \sin(\theta_r))) / (J_{az} * R_m)
 \end{aligned}$$

$$\begin{aligned}
 h_2(\theta) = & (\omega_{iby}^b * \cos^2(\theta_p) * (J_{ay} + J_{py}) + (J_{rx} \\
 & - J_{rz}) * (\omega_{ibx}^b * \cos(\theta_r) + \omega_{ibz}^b \\
 & * \sin(\theta_r)) * (\omega_{ibz}^b * \cos(\theta_r) \\
 & - \omega_{ibx}^b * \sin(\theta_r)) - \sin(\theta_p) \\
 & * (\cos(\theta_p) * (\omega_{ibz}^b * \cos(\theta_r) \\
 & - \omega_{ibx}^b * \sin(\theta_r)) - \omega_{iby}^b \\
 & * \sin(\theta_p)) * (J_{az} + J_{pz}) \\
 & + (\omega_{ibx}^b * \cos(\theta_r) + \omega_{ibz}^b \\
 & * \sin(\theta_r)) * (\omega_{ibz}^b * \cos(\theta_r) \\
 & - \omega_{ibx}^b * \sin(\theta_r)) * (J_{ax} + J_{px}) \\
 & - \cos(\theta_p) * (\cos(\theta_p) * (\omega_{ibz}^b \\
 & * \cos(\theta_r) - \omega_{ibx}^b * \sin(\theta_r)) \\
 & - \omega_{iby}^b * \sin(\theta_p)) * (\omega_{ibx}^b \\
 & * \cos(\theta_r) + \omega_{ibz}^b * \sin(\theta_r)) \\
 & * (J_{az} + J_{pz}) - \sin(\theta_p) \\
 & * (\sin(\theta_p) * (\omega_{ibz}^b * \cos(\theta_r) \\
 & - \omega_{ibx}^b * \sin(\theta_r))
 \end{aligned}$$

(60)

$$\begin{aligned}
& + \omega_{iby}^b * \cos(\theta_p) * (\omega_{ibx}^b * \cos(\theta_r) + \omega_{ibz}^b \\
& \quad * \sin(\theta_r)) * (J_{ay} + J_{py}) \\
& + \cos(\theta_p) * \sin(\theta_p) * (\omega_{ibz}^b \\
& \quad * \cos(\theta_r) - \omega_{ibx}^b * \sin(\theta_r)) \\
& \quad * (J_{ay} + J_{py}) / (J_{ay} + J_{py}) \\
& \quad * \cos^2(\theta_p) + J_{ry}) \\
& + (T_{dr} + N * T_{am}) / (J_{ay} + J_{py}) * \cos^2(\theta_p) \\
& \quad + J_{ry}) + (J_m * N * \dot{\omega}_{iby}^b * (N \\
& \quad - 1)) / (J_{ay} + J_{py}) * \cos^2(\theta_p) \\
& \quad + J_{ry}) + (K_e * K_t * N^2 \\
& \quad * \omega_{iby}^b) / (R_m * (J_{ay} + J_{py}) \\
& \quad * \cos^2(\theta_p) + J_{ry})
\end{aligned}$$

CREDIT AUTHORSHIP CONTRIBUTION STATEMENT

Mohammad Mehdi Zohrei: Conceptualization, Funding acquisition, Investigation, Project administration, Roles/Writing - original draft, Writing - review & editing. **Hamidreza Javanmardi:** Data curation, Formal analysis, Investigation, Methodology, Resources, Software, Supervision, Validation, Visualization, Writing - review & editing.

DECLARATION OF COMPETING INTEREST

The authors declare that they have no known competing financial interests or personal relationships that could have appeared to influence the work reported in this paper. The ethical issues; including plagiarism, informed consent, misconduct, data fabrication and/or falsification, double publication and/or submission, redundancy has been completely observed by the authors.

REFERENCES

- [1] A. Altan, and R. Hacıoğlu, "Model predictive control of three-axis gimbal system mounted on UAV for real-time target tracking under external disturbances," *Mechanical Systems and Signal Processing*, vol. 138, p. 106548, 2020.
- [2] J. Mao, J. Yang, X. Liu, S. Li, and Q. Li, "Modeling and robust continuous TSM control for an inertially stabilized platform with couplings," *IEEE Transactions on Control Systems Technology*, vol. 28, no. 6, pp. 2548–2555, 2020.
- [3] M. M. Zohrei, A. Roosta, and B. Safarinejadian, "Robust backstepping control based on neural network stochastic constrained for three axes inertial stable platform," *Journal of Aerospace Engineering*, vol. 35, no. 1, p. 04021117, 2022.
- [4] W. M. Abdel-Wahab et al., "Affordable large scale active-phased array antenna for Ka-band mobile SATCOM applications," in *2019 13th European Conference on Antennas and Propagation (EuCAP)*, 2019, pp. 1–4.
- [5] D.-H. Lee, D.-Q. Tran, Y.-B. Kim, and S. Chakir, "A robust double active control system design for disturbance suppression of a two-axis gimbal system," *Electronics*, vol. 9, no. 10, article 10, 2020.
- [6] C. D. Rodin, F. A. de Alcantara Andrade, A. R. Hovenburg, T. A. Johansen. "A survey of practical design considerations of optical imaging stabilization systems for small unmanned aerial systems," *Sensors*, vol. 19, no.21, p.4800, 2019.
- [7] V. Rosas-Cervantes, and S.-G. Lee, "3D localization of a mobile robot by using Monte Carlo algorithm and 2D features of 3D point cloud," *Int. J. Control Autom. Syst.*, vol. 18, no. 11, pp. 2955–2965, 2020.
- [8] Y. Zou, and X. Lei, "A compound control method based on the adaptive neural network and sliding mode control for inertial stable platform," *Neurocomputing*, vol. 155, pp. 286–294, 2015.
- [9] S. Cong, K. Deng, W. Shang, D. Kong, and H. Shen, "Isolation control for inertially stabilized platform based on nonlinear friction compensation," *Nonlinear Dyn*, vol. 84, no. 3, pp. 1123–1133, 2016.
- [10] S. Liu, H. Che, and L. Sun, "Research on stabilizing and tracking control system of tracking and sighting pod," *J. Control Theory Appl.*, vol. 10, no. 1, pp. 107–112, Feb. 2012.
- [11] M. Khayatian, and M. Arefi, "Adaptive dynamic surface control of a two axis gimbal system," *IET Science, Measurement & Technology*, vol. 10, 2016.
- [12] Y. Zhang et al., "Fuzzy-PID control for the position loop of aerial inertially stabilized platform," *Aerospace Science and Technology*, vol. 36, pp. 21–26, 2014,
- [13] F. Liu, H. Wang, Q. Shi, H. Wang, M. Zhang, and H. Zhao, "Comparison of an ANFIS and Fuzzy PID control model for performance in a two-axis inertial stabilized platform," *IEEE Access*, vol. 5, pp. 12951–12962, 2017.
- [14] M. Davanipour, H. Javanmardi, and N. Goodarzi, "Chaotic self-tuning PID controller based on Fuzzy wavelet neural network model," *Iran J Sci Technol Trans Electr Eng*, vol. 42, no. 3, pp. 357–366, 2018.
- [15] P. Setoodeh, A. Khayatian, and E. Farjah, "Backstepping-based control of a strapdown boatboard camera stabilizer," *International Journal of Control Automation and Systems*, vol. 5, pp. 15–23, 2007.
- [16] H. Javanmardi, M. Dehghani, M. Mohammadi, N. Vafamand, and T. Dragičević, "Optimal frequency regulation in AC mobile power grids exploiting bilinear matrix inequalities," *IEEE Transactions on Transportation Electrification*, pp. 1–1, 2021.
- [17] S. Pan, Y. Wu, J. Zhang, S. Zhou, and H. Zhu, "Modeling and control of a 2-degree-of-freedom gyro-stabilized platform driven by ultrasonic motors," *Journal of Intelligent Material Systems and Structures*, vol. 29, no. 11, pp. 2324–2332, 2018.
- [18] C. Yu, A. Li, S. Zhang, and X. Bai, "Robust finite time second-order sliding mode stabilization control for floated inertial platform," in *Proceedings of the Institution of Mechanical Engineers, Part G: Journal of Aerospace Engineering*, vol. 232, no. 9, pp. 1620–1627, 2018.
- [19] H. Javanmardi, M. Dehghani, M. Mohammadi, S. Siamak, and M. R. Hesamzadeh, "BMI-Based load frequency control in microgrids under false data injection attacks," *IEEE Systems Journal*, pp. 1–11, 2021.
- [20] W. A. Pradana, E. Joelianto, A. Budiyo, and W. Adiprawita, "Robust MIMO H ∞ integral-backstepping

- PID controller for hovering control of unmanned model helicopter," *Journal of Aerospace Engineering*, vol. 24, no. 4, pp. 454–462, 2011.
- [21] Z. Xiangyang, L. Xinyue, and Y. Chao, "Disturbances rejection based on robust H_∞ control for an aerial inertially stabilized platform," in *2019 14th IEEE International Conference on Electronic Measurement Instruments (ICEMI)*, 2019, pp. 1396–1401.
- [22] H. Javanmardi, M. Dehghani, M. Mohammadi, and M. R. Hesamzadeh, "A mesh-based partitioning algorithm for decreasing conservatism in solving bilinear matrix inequality problems," *Optimal Control Applications and Methods*, 2023.
- [23] H. R. Javanmardi, M. Dehghani, A. A. Safavi, and R. Abolpour, "Model predictive control of a class of uncertain nonlinear discrete time systems: The LMI approach," in *2016 24th Iranian Conference on Electrical Engineering (ICEE)*, 2016, pp. 323–328.
- [24] X. Zhou, Y. Shi, L. Li, R. Yu, and L. Zhao, "A high precision compound control scheme based on non-singular terminal sliding mode and extended state observer for an aerial inertially stabilized platform," *Int. J. Control Autom. Syst.*, vol. 18, no. 6, pp. 1498–1509, 2020.
- [25] F. Dong, X. Lei, and W. Chou, "A Dynamic model and control method for a two-axis inertially stabilized platform," *IEEE Transactions on Industrial Electronics*, vol. 64, no. 1, pp. 432–439, 2017.
- [26] H. Ramirez-Rodriguez, V. Parra-Vega, A. Sanchez-Orta, and O. Garcia-Salazar, "Robust backstepping control based on integral sliding modes for tracking of quadrotors," *J Intell Robot Syst*, vol. 73, no. 1, pp. 51–66, 2014.
- [27] C. Afri, V. Andrieu, L. Bako, and P. Dufour, "State and parameter estimation: A nonlinear luenberger observer approach," *IEEE Transactions on Automatic Control*, vol. 62, no. 2, pp. 973–980, 2017.
- [28] S. Lee and S. Jung, "An observer design technique for improving velocity estimation of a gimbal system," in *International Conference on Robot Intelligence Technology and Applications*, Springer, 2017, pp. 337–343.
- [29] N. Reichbach and A. Kuperman, "Recursive-Least-squares-based real-time estimation of supercapacitor parameters," *IEEE Transactions on Energy Conversion*, vol. 31, no. 2, pp. 810–812, 2016.
- [30] X. Lei, Y. Zou, and F. Dong, "A composite control method based on the adaptive RBFNN feedback control and the ESO for two-axis inertially stabilized platforms," *ISA Transactions*, vol. 59, pp. 424–433, 2015.
- [31] Z.-L. Zhao, and B.-Z. Guo, "A novel extended state observer for output tracking of MIMO systems with mismatched uncertainty," *IEEE Transactions on Automatic Control*, vol. 63, no. 1, pp. 211–218, 2018.
- [32] A. Grovlen and T. I. Fossen, "Nonlinear control of dynamic positioned ships using only position feedback: an observer backstepping approach," in *Proceedings of 35th IEEE Conference on Decision and Control*, Dec. 1996, vol.3. pp. 3388–3393.
- [33] I. Hosseini, M. Mirzaei, and M. H. Asemani, "Nonlinear output feedback for HL-20 flight control using back-stepping observer," *J Intell Robot Syst*, vol. 100, no. 3, pp. 1401–1416, 2020.
- [34] J. Valasek, and W. Chen, "Observer/Kalman filter identification for online system identification of aircraft," *Journal of Guidance, Control, and Dynamics*, vol. 26, no. 2, pp. 347–353, 2003.
- [35] A. F. Taha, A. Elmahdi, J. H. Panchal, and D. Sun, "Unknown input observer design and analysis for networked control systems," *International Journal of Control*, vol. 88, no. 5, pp. 920–934, 2015.
- [36] M. Liu, L. Zhang, P. Shi, and H. R. Karimi, "Robust control of stochastic systems against bounded disturbances with application to flight control," *IEEE Transactions on Industrial Electronics*, vol. 61, no. 3, pp. 1504–1515, 2014.
- [37] M. Pourgholi, and V. J. Majd, "A new non-fragile H_∞ proportional—integral filtered-error adaptive observer for a class of non-linear systems and its application to synchronous generators," in *Proceedings of the Institution of Mechanical Engineers, Part I: Journal of Systems and Control Engineering*, vol. 225, no. 1, pp. 99–112, 2011.
- [38] M. Pourgholi, and V. J. Majd, "A nonlinear adaptive resilient observer design for a class of Lipschitz systems using LMI," *Circuits Syst Signal Process*, vol. 30, no. 6, pp. 1401–1415, 2011.
- [39] M. Mirzaei, I. Hosseini, and V. Ghaffari, "MEMS gyroscope fault detection and elimination for an underwater robot using the combination of smooth switching and dynamic redundancy method," *Microelectronics Reliability*, vol. 109, p. 113677, 2020.
- [40] H. K. Khalil, *Nonlinear Systems*. Prentice Hall, 2002.
- [41] T. S. Shores, "Applied linear algebra and matrix analysis," in *Undergraduate Texts in Mathematics*. New York: Springer-Verlag, 2007.

BIOGRAPHY

Mohammad Mehdi Zohrei received his B. Sc. and M. Sc. degrees in Electrical Engineering from Shiraz University, Shiraz, Iran, in 1998 and 2003, respectively and his PhD from Shiraz University of Technology, Shiraz, Iran in 2022. He is interested include Inertially Stabilized Platform, Three degrees of freedom stabilizer, Nonlinear control approaches in ISP



Control.



Amidreza Javanmardi received his B. Sc. and M. Sc. degrees in Electrical Engineering from Shiraz University, Shiraz, Iran, in 2013 and 2015, respectively and her PhD from Shiraz University, Shiraz, Iran in 2021. He is interested include Bilinear Matrix Inequality (BMI) applications in control, Model Predictive Control (MPC), automation and instruments, robotic and artificial intelligence.

Copyrights

© 2024 Licensee Shahid Chamran University of Ahvaz, Ahvaz, Iran. This article is an open-access article distributed under the terms and conditions of the Creative Commons Attribution –Non-Commercial 4.0 International (CC BY-NC 4.0) License (<http://creativecommons.org/licenses/by-nc/4.0/>).

